A robust nanofluidic membrane with tunable zero-order release for implantable dose specific drug delivery†

Daniel Fine,‡[a] Alessandro Grattoni,‡[a] Sharath Hosali,[b] Arturas Ziemys,[a] Enrica De Rosa,[a] Jaskaran Gill,[a] Ryan Medema,[b] Lee Hudson,[b] Milos Kojic,[a] Miljan Milosevic,[c] Louis Brousseau III,[a] Randy Goodall,[b] Mauro Ferrari*[ade] and Xuewu Liu*[a]

Received 10th May 2010, Accepted 14th July 2010
DOI: 10.1039/c0lc00013b

This manuscript demonstrates a mechanically robust implantable nanofluidic membrane capable of tunable long-term zero-order release of therapeutic agents in ranges relevant for clinical applications. The membrane, with nanochannels as small as 5 nm, allows for the independent control of both dosage and mechanical strength through the integration of high-density short nanochannels parallel to the membrane surface with perpendicular micro- and macrochannels for interfacing with the ambient solutions. These nanofluidic membranes are created using precision silicon fabrication techniques on silicon-on-insulator substrates enabling exquisite control over the monodispersed nanochannel dimensions and surface roughness. Zero-order release of analytes is achieved by exploiting molecule to surface interactions which dominate diffusive transport when fluids are confined to the nanoscale. In this study we investigate the nanofluidic membrane performance using custom diffusion and gas testing apparatuses to quantify molecular release rate and process uniformity as well as mechanical strength using a gas based burst test. The kinetics of the constrained zero-order release is probed with molecules presenting a range of sizes, charge states, and structural conformations. Finally, an optimal ratio of the molecular hydrodynamic diameter to the nanochannel dimension is determined to assure zero-order release for each tested molecule.

Introduction

Nanoscale fluidic devices have been investigated as a promising long-term zero-order continuous release technology for therapeutic applications for over a decade.[1–3] The zero-order release is made possible by the constrained diffusion resulting from 2-dimensional nanoscale confinement and consequent domination of molecule to surface interactions.[4–9] These architectures can be integrated with a wide range of reservoir geometries, have no moving or electronic components, and have tunable release rates, independent of the concentration of drug in the reservoir, by modulation of the size and number of the nanochannels. Nanofluidic platforms offer an important therapeutic alternative to pulsatile delivery[10,11] and compare very favorably to other continuous release technologies such as biodegradable polymers[12] and osmotic[13] and electroosmotic pumps.[14,15] Many different materials have been used to generate nanochannels and nanopores, including silicon,[16–19] silica,[20] alumina,[21,22] silicon nitride,[23] carbon,[24] titanium dioxide,[25] polydimethylsiloxane,[26,27] SU-8,[28] and gold,[29] along with an array of techniques for their manufacturing.[16,20,30–35]

Silicon fabrication techniques developed for the production of microprocessors constitutes an important set of tools for manufacturing nanochannel devices for drug delivery given the required precision, accuracy, throughput, and reliability necessary for many clinically relevant dosing regimens.[36] Many of the materials compatible with silicon manufacturing have also been demonstrated to be biocompatible.[37,38] Nanochannel membranes produced using silicon fabrication techniques were first investigated for possible clinical applications in immunoisolating biocapsules, capable of maintaining the viability of pancreatic islets of Langerhans both *in vitro* and *in vivo*.[39,40] They were then adapted for direct drug delivery platforms to release glucose, interferon, and bovine serum albumin (BSA)[2,3,41] as well as for hemofiltration for possible use in artificial kidneys.[42,43] These membranes possess highly ordered nanochannels that prevent significant protein adsorption and mineralization, a problem for both organic and inorganic materials with more chaotic nanostructure.[44,45] In addition to a lack of biofouling, Walczak *et al.* also showed the release rates were stable for up to 6 months *in vivo* and were unaffected by tissue encapsulation for the molecules tested (around 14.4kDa in size at rates in the tens of μg/day).[46] Furthermore, several surface functionalizations have been investigated to reduce undesirable protein adsorption.[47–49]

Previous implementations of silicon based nanochannel drug delivery membranes were fabricated either with nanochannels perpendicular to the membrane surface, by means of a sacrificial oxide,[16,17,19] or sandwiched horizontally between two bonded bulk substrates (silicon, Pyrex, *etc.*).[18,41] Given the direct

[a]*Department of Nanomedicine and Biomedical Engineering, The University of Texas Health Science Center at Houston, Houston, TX, 77030, USA. E-mail: Mauro.ferrari@uth.tmc.edu; Xuewu.liu@uth.tmc.edu*
[b]*Nanomedical Systems, Inc., Austin, TX, 78741, USA*
[c]*R & D Center for Bioengineering, Sretenjskog Ustava, 34000 Serbia Kragujevac*
[d]*The University of Texas M. D. Anderson Cancer Center, Houston, TX, 77030, USA*
[e]*Rice University, Houston, TX, 77005, USA*
† Electronic supplementary information (ESI) available: Supplementary information. See DOI: 10.1039/c0lc00013b
‡ equal contribution

relationship between nanochannel length and membrane thickness, membranes with perpendicular nanochannels suffered from poor mechanical stability as short nanochannels required thin membranes.[40] Restrictions on the nanochannel length were due to process related nanochannel aspect ratio limitations, a problem that could be alleviated by new fabrication methods,[50] as well as the low release rates which resulted from the increased transit times of molecules diffusing through longer nanochannels. Furthermore, it was difficult to control the surface roughness of the vertically oriented channels because part of the nanochannel surface was polysilicon, comprised of crystalline grains separated by grain boundaries, as opposed to single crystal silicon. To improve the mechanical stability and minimize the channel surface roughness the sandwiched bulk membranes were adapted for drug delivery but presented an extremely low release rate.[3] In this architecture, the nanochannels were connected to the inlet and outlet ports of the membrane by an extensive network of long fingered horizontal microchannels resulting in insufficient nanochannel densities and a low overall fluidic channel cross section.

Here we present a solution to both of the aforementioned delivery problems with a mechanically robust nanofluidic platform, the nanochannel delivery system (nDS), capable of the tunable zero-order release of therapeutic molecules in ranges of clinical significance. The structural complexity of this architecture is derived from the integration of conventional silicon fabrication processes and silicon-on-insulator (SOI) substrates. The nanochannels in this architecture are horizontally oriented and sandwiched between the SOI device layer and a thin bonded or chemical vapor deposited dielectric cap with vertically integrated microchannels. This takes advantage of the easily variable nanochannel lengths and low channel surface roughness of the aforementioned sandwiched bulk membrane design while allowing for the higher nanochannel density and shorter molecular transit times (higher release rates) of the perpendicular nanochannel membrane. The handle wafer of the SOI is used to provide the robust mechanical support. The nDS membranes were gas tested to quantify both process uniformity and mechanical strength. Five molecules were selected for the analysis of diffusive transport through the membranes based on their size, charge, and shape: glucose, fluorescein isothiocyanate conjugated dextran (FITC-dextran), dendritic fullerene 1 (DF-1), interferon α-2b (INFα-2b) and bovine serum albumin (BSA). The experimental data were compared to analytical and finite element modeling predictions to investigate the extent of the nanoconfinement effect. Finally, an optimum molecular hydrodynamic diameter-to-nanochannel height ratio of approximately 1 : 3 was determined to guarantee the zero-order release of the selected molecules.

Experimental details

Nanofluidic membrane fabrication

The nDS membranes (see Fig. 1) used in this study were designed to have identical structures but had nanochannels fabricated using two different techniques in order to characterize the effect of process on mechanical integrity: anodic bonding of membrane layers versus sacrificial nanochannel formation of assembled

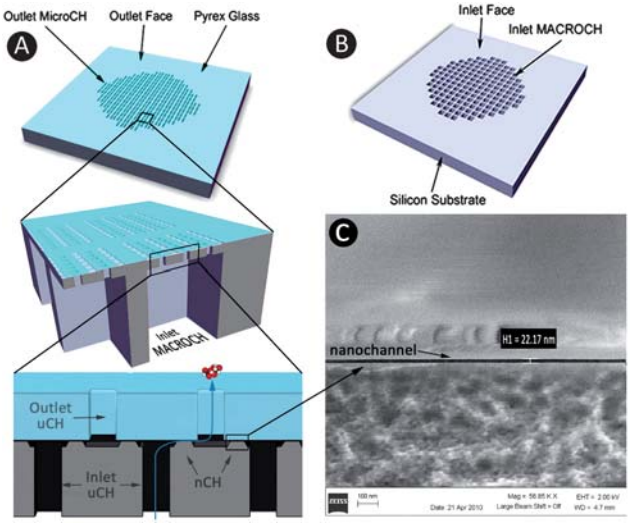

Fig. 1 A-B) present schematic representations of a nanoscale delivery system (nDS) membrane. C) is a scanning electron micrograph of the nanochannel outlet of the nDS. The nanochannel was imaged by fracturing an nDS membrane using a mechanical clamp.

layers. The membranes are fabricated using the complete thickness of silicon-on-insulator (SOI) substrates with a 30 μm device layer, a 400 nm or 1μm buried oxide, and a 500 or 700 μm handle wafer. Micron length nanochannels of 5, 13, or 22 nm in depth are formed in the plane of the SOI substrate to connect 5 μm square inlet/outlet ports formed in the device layer/capping dielectric respectively. The inlet microchannels are accessed *via* 200 by 200 μm openings through the SOI handle wafer. Each opening in the handle wafer connects multiple inlet channels, which each address multiple nanochannels. While the specific dimensions noted above were fabricated for this set of experiments, the technique is fully flexible; extremely precise dimensions and tolerances can be set over a wide range for both microchannels (±100 nm) and nanochannels (±1 nm) to support target applications.

Anodically bonded nDS chips

The fabrication process for anodically bonded nDS chips (nDS*ab*), with a total of 77,280 nanochannels, is shown in Fig. 2. First, a series of nanotrenches 5 μm wide, 205 μm long, 22 nm deep, and separated by 3 μm was patterned on the surface of the device layer of a SOI substrate (Silicon Quest International, Inc., Santa Clara, California, USA) by selective dry oxidation through a 65 nm thick silicon nitride masking layer using a CHF_3/O_2 plasma (Fig. 2. A and C). The silicon nitride masking layer was deposited by low pressure chemical vapor deposition (LPCVD) onto a 65 nm thick silicon dioxide pad layer grown by dry thermal oxidation. The pad oxide thickness was selected to insure the anisotropic dry etch of the silicon nitride windows would not breach the substrate surface and was etched using a buffered oxide etch (BOE) to remove the remaining oxide from inside the pattern. After the oxidation of the nanotrenches was complete, both the nitride and the selectively grown oxide were stripped in dilute hydrofluoric acid (HF).

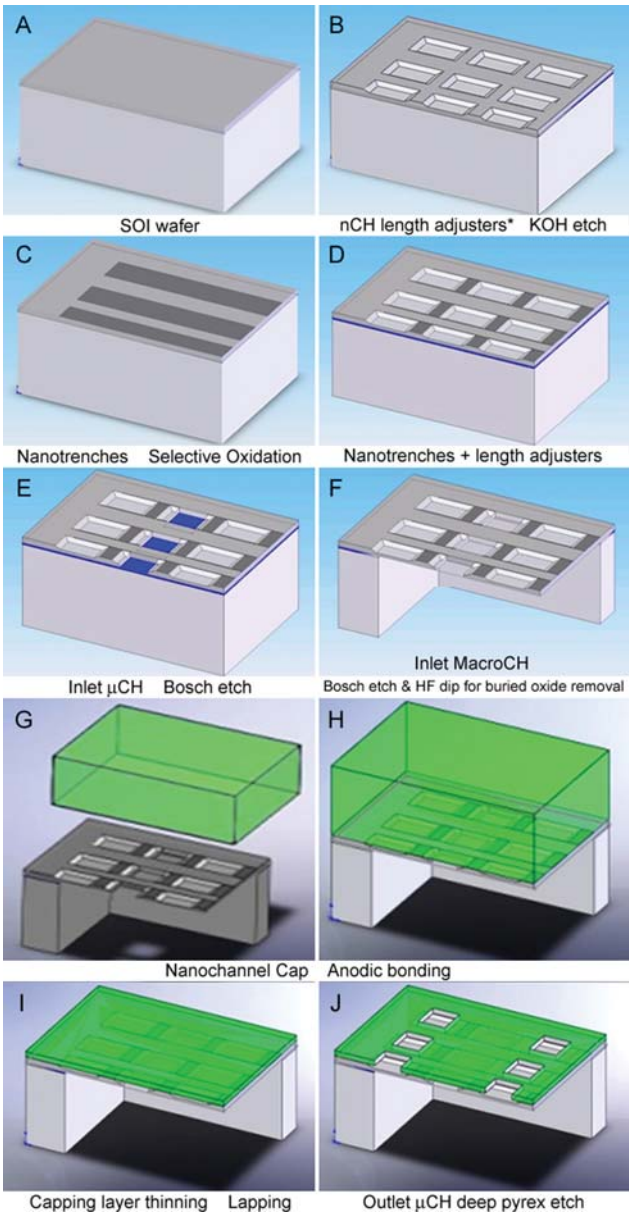

Fig. 2 The fabrication process flow for the anodically bonded nanoscale delivery membrane. * indicates an optional process step. See text and ESI† for process details.

Both sides of the wafer were then masked with 1 μm of LPCVD SiO_2. The front side oxide was thinned to 400 nm using a CHF_3/O_2 plasma etch, then the 5 μm inlet channels were lithographically defined and similarly dry etched. The access macrochannels through the handle wafer were patterned using back-side alignment photolithography and CHF_3/O_2 plasma etch. Following the transfer of the inlet micro- and macrochannel patterns into the hard mask, the resist was stripped using a Piranha clean and the substrate briefly dipped in dilute HF to remove any chemically grown oxide from the exposed silicon surfaces. The patterns were then etched into the silicon, first the inlet microchannels and then the inlet macrochannels, down to the 400 nm buried oxide layer using the Bosch process[51] (Fig. 2. E and F). After completing the Bosch etch for both patterns, the remaining oxide hard mask as well as the exposed buried oxide through the macrochannels was removed in dilute HF. At this point the nanotrench depth and surface roughness was measured by atomic force microscopy (AFM) at 11 points over the device layer surface (see ESI†).

The nanochannels were formed from the nanotrenches by capping the nanotrenches with a 500 μm thick anodically bonded Pyrex 7740 borosilicate glass wafer 100 mm in diameter (Fig. 2. G and H). The Pyrex capping wafer was then lapped with a (nominally) 15 μm diamond particulate slurry followed by a cerium oxide final polish to a final thickness of around 20 μm, as measure by reflectometry (Fig. 2. I). Following the Pyrex lapping, 5 by 5μm square outlet microchannels were dry etched through the Pyrex[52] by first depositing a seed layer of 10 nm of chromium/50 nm of gold by electron beam evaporation followed by the patterning of 5 μm square mesas in positive resist. These mesas template the electrochemical deposition of nickel to a thickness of 4μm which was used as a hard mask for the Pyrex dry etch. The resist mesas were stripped and the seed layer was wet etched to expose the Pyrex for etching of the outlets (Fig. 2. J). The outlet microchannels were over etched to insure that the nanochannels or nanochannel length adjusters were effectively interfaced. The nickel mask was stripped using a wet etch and individual membranes separated by dicing the wafer into die.

Nanofluidic membranes with shorter effective nanochannel lengths were also produced by the use of length adjusters etched into the device layer surface prior to the nanotrench fabrication (see Fig. 2. B and D). These allowed for final effective nanochannel lengths of 0.5 to 3 μm. A detailed list of process specifics for this fabrication flow can be found in the ESI.†

Sacrificial layer nDS chips

A second fabrication process was developed which supports volume scale-up, increased precision and reproducibility in setting the nanochannel height, and a wider array of advanced material options. This process generates membranes with the same nanofluidic structure as the nDS*ab* but 5 and 13 nm nanochannels and is referred to as the sacrificial layer nDS chip (nDS*sl*). These membranes were designed with 288,834 nanochannels. Briefly, a 200 mm SOI wafer with a 30 μm device layer, a 1 μm buried oxide layer, and a 700 μm handle wafer was first coated with a sacrificial metal layer to the desired nanochannel thickness and top coated with a thin layer of silicon nitride. Inlet microchannels were patterned and the silicon nitride/sacrificial metal stack was dry etched using a CF4/Ar/O2 plasma, followed by a Bosch etch of the device layer, stopping on the buried oxide. These inlet microchannels were then plugged and planarized (CMP) using a sacrificial material. The nanochannel pattern was transferred into the silicon nitride and sacrificial layers through plasma etch leaving behind a surface covered with nanochannel lines (as opposed to trenches in the previous case) and inlet microchannels. A thick layer of silicon nitride was then deposited on this surface through which outlet microchannels of 3×3 μm were slightly over-etched using CF4/Ar/O2 plasma, to ensure the nanochannels were properly connected. As in the other process, back-side alignment lithography and Bosch etch were used to open access macrochannels through the handle wafer to the inlet

microchannels. The exposed buried oxide layer was subsequently removed by dry plasma etch. Finally, to form the nanochannels, the sacrificial nanochannel layer and the materials in the inlet microchannel plugs were removed with appropriate etchants.

Testing apparatus

The gas testing system

Convective nitrogen flow (at 0.3 MPa) was used to characterize the membranes for structural integrity, called the burst test, and the reproducibility of the fabrication protocol. For this purpose, a modified version of the gas testing apparatus used in our previous work was developed.[53] With this system, the time constant D, representative of the fluidic characteristic of the membranes, was obtained for each nDS. Additionally, high pressure testing (up to 4.1 MPa) was performed to evaluate the mechanical strength and stability of the chip. In this context, the fluidic characteristic curve (fcc) was first measured prior to the high pressure test. The membranes were then exposed to overpressure in increments of 1.38 MPa with the fcc measured after each increment. (see ESI† for additional information).

The diffusion testing system

The passive diffusive transport characteristics of the nDS membranes were evaluated using two custom diffusion testing devices, as shown in Fig. 3. The devices are composed of stainless steel 316L bodies housing drug and sink solution reservoirs. The reservoirs are separated by the nDS chip which is sealed in its housing by means of two silicon rubber o-rings. The first diffusion device (D1) presents a 300μL drug solution reservoir and a 4.32 mL sink reservoir which is obtained by bonding one metal body to a UV macro-cuvette through an UV-curing epoxy resin. The D1 enables the direct measurement of the concentration of an absorbing species diffusing through the nanochannels by means of UV/Vis spectrophotometry. The second device D2 was developed for molecules requiring direct sampling from the sink solution to measure concentration. For this reason the reservoirs, with a maximum volume of 300 μL, are accessible *via* a silicon rubber septa for periodic removal of sink solution and replenishment with fresh buffer.

Selection of diffusing species

Glucose

Glucose (Sigma-Aldrich Inc., MW 180.16) presents a hydrodynamic diameter of 0.5 nm, and neutral net charge. 280 μL of a 2.75 M glucose solution containing 0.05% sodium azide (Sigma-Aldrich Inc.) was loaded into the source reservoir and 155 μL of DI water + 0.05% sodium azide was loaded into the sink reservoir of the D2 device. Six replicates were performed for nDS*sl* membranes with nanochannels 5 nm in height and 1 μm long. The glucose concentration was determined from a 150 μL solution aliquot removed from the sink reservoir and replaced with an equal amount of fresh DI water plus 0.05% sodium azide at intervals of approximately 24 h. A FreeStyle Lite® Blood Glucose Monitoring System was used to measure the glucose concentration. The device was calibrated with standard solutions

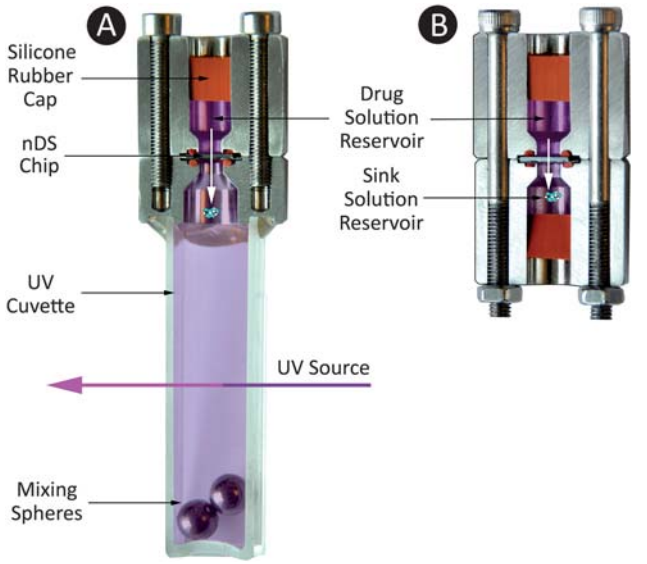

Fig. 3 Pictures of the cross sections of the custom diffusion devices. A) The UV-Vis diffusion chamber D1 which allows for direct quantification of the amount released and therefore represents a closed system. B) The sampling diffusion device D2 which requires the sink reservoir to be directly sampled to quantify release.

within its measurement range of 20 to 500 mg/mL. A control experiment performed using a bulk silicon chip with no nanochannels showed no transport of glucose (*i.e.* no leaks in the system).

FITC-dextran

Fluorescein isothiocyanate conjugated dextran (FITC-dextran) (Molecular Probes®, Invitrogen Corp. MW 10 kDa) has an equivalent hydrodynamic diameter of 6 nm, and a negative net charge of −1e (at a pH of 7) originating from the fluorescein. For each of 5 replicates, 300 μL of a 5mg/mL solution of FITC-dextran in standard phosphate buffer solution (PBS, GIBCO™, Invitrogen Corp., pH 7.4) was loaded into the source reservoir and 250μL of PBS loaded into the sink reservoir of the D2 device. nDS*ab* membranes with nanochannels 22 nm in height were used. A 200 μL aliquot removed from the sink reservoir and replaced by an equal amount of fresh PBS was repeated each 2 to 3 days. The FITC-dextran concentration was determined by comparison to a calibration curve using an UV/Vis spectrophotometer with an excitation wavelength of 485 nm and a measurement wavelength of 520 nm.

BSA, DF-1, INFα-2b

The transport of BSA (Sigma-Aldrich Inc., MW 66 kDa, hydrodynamic diameter = 5.5 nm, negative net charge = −17e at pH 7), DF-1 (ChemPacific, Baltimore, MD, MW 2810.6 Da, hydrodynamic diameter = 2.5 nm, negative net charge = −18e at pH 7) and INFα-2b (Cell Sciences, Inc., Canton, MA, MW 19 kDa, hydrodynamic diameter = 3.2 nm, negative net charge = −2e at pH 7) was characterized by UV absorption in the D1 device. A calibration curve was generated for each molecule in standard PBS using a UV/Vis spectrophotometer

(Beckman Coulter, Inc., DU 730) at wavelengths of 228 nm (BSA), 320 nm (DF-1) and 230 nm (INFα-2b). The UV cuvette sink reservoirs in all of these experiments were loaded with 4.32 mL of PBS. For BSA, a total of 7 replicates were prepared using nDS*ab* membranes with nanochannels 22 nm in height and 2 um long and source reservoirs loaded with 150 μL of both 20 mg/mL (4 replicates) and 40 mg/mL (3 replicates) solutions of BSA in PBS. For DF-1, a total of 6 replicates were tested using nDS*sl* membranes with nanochannels of both 5 nm (3 replicates) and 13 nm (3 replicates) in height and 1 μm long and source reservoirs loaded with 270 μL of a 2 mg/mL solution of DF-1 in PBS. For INFα-2b a total of 3 replicates were tested using nDS*sl* membranes with nanochannels of 13nm in height and 1 μm long and source reservoirs loaded with 150 μL of a 1 mg/mL solution of INFα-2b in PBS.

Results

The AFM characterization performed during the fabrication of the nDS*ab* showed channel heights of 22.6 ± 2.2% with a surface roughness at the bottom of the channel of 0.270 ± 0.58nm-rms. All membranes were visually inspected through optical microscopy. 19 defective nDSab were discarded from the entire wafer (100 nDS). Gas testing characterization was then performed on the remaining 81 chips. The histogram in Fig. 4A) shows the distribution of the population of data related to the characteristic time constant D obtained for each membrane (see ESI†). 57 membranes produced time constants in a range of approximately one order of magnitude. Grattoni *et al.* previously demonstrated that gas fluidics is one order of magnitude more sensitive to structural variation then diffusive transport, implying that this wafer had a yield of over 50%.[53] Burst testing results for an nDS*ab* are shown in Fig. 4B). The membrane was able to withstand gas pressures in excess of 2.76 MPa with no appreciable variation in the gas flow dynamics detected after pressure increments that did not lead to catastrophic breakdown. The nDS*sl* membranes, owing to a thicker handle wafer, were able to routinely reach the burst test detection pressure limit of 4.1 MPa with a similar lack of pressure induced dynamic flow variation.

Fig. 5 shows the experimental diffusion results for DF-1, glucose, FITC-dextran, BSA, and interferon along with the theoretical predictions of unconstrained Fickian diffusion. For the FITC-dextran, BSA and INFα-2b results, linear regressions are also plotted. For BSA, the linear fit is depicted after the constrained release has stabilized (this phenomena will be discussed later). The analytical calculations of the Fickian release were based on the relation[54]:

$$Q_A(t) = \left(C^0_{A1} - C^0_{A2}\right) V_1 \frac{V_2}{V_1 + V_2}\left(1 - e^{-\lambda A t}\right) \quad (1)$$

$$\lambda_A = \frac{D_{AB} S}{V_1 L}\left(1 + \frac{V_1}{V_2}\right) \quad (2)$$

where $Q_A(t)$ is the amount of analyte released, c^0_{A1} and c^0_{A2} are the starting concentrations in the source and sink reservoirs, V_1 and V_2 are the source and sink volumes, D_{AB} is the bulk diffusion coefficient (listed in Table 2), L is the channel length, S is the channel cross section, and t is the elapsed time. As the sink reservoirs for the FITC-dextran diffusion testing were sampled and refreshed for each time point, eqn (1) was used iteratively to simulate the sink fluid sampling at the specific time-points. A Finite Element Analysis (FEA) of the nDS membrane was developed and used to predict the Fickian release profile of glucose (see ESI†). The FEA prediction was numerically calculated by using glucose diffusivity as a function of the concentration and also appropriately handled sampling effects. Experimental conditions and release rates for each molecule are shown in Fig. 5.

Discussion

The major advantages of this nDS platform, in addition to those enumerated earlier for silicon fabricated nanofluidic systems in general, are its structural and operational adaptability. This is possible because the nanochannel length is not a function of the membrane thickness, with nanochannels machined parallel and micro- and macrochannels perpendicular to the substrate surface. The fabrication process allows for the

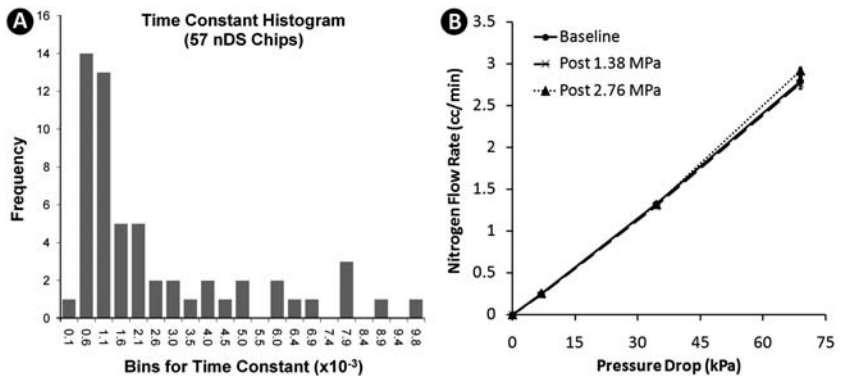

Fig. 4 A) Histogram representing the distribution of time constants from membranes obtained from a single wafer. The range of time constants is approximately one order of magnitude. B) The gas fluidic characteristic curves recorded for a single nDS*ab* after exposure to a sequence of overpressures during burst testing. Based on these results, no degradation of the mass transport properties of the membrane was detected after overpressure exposure prior to catastrophic membrane breakdown.

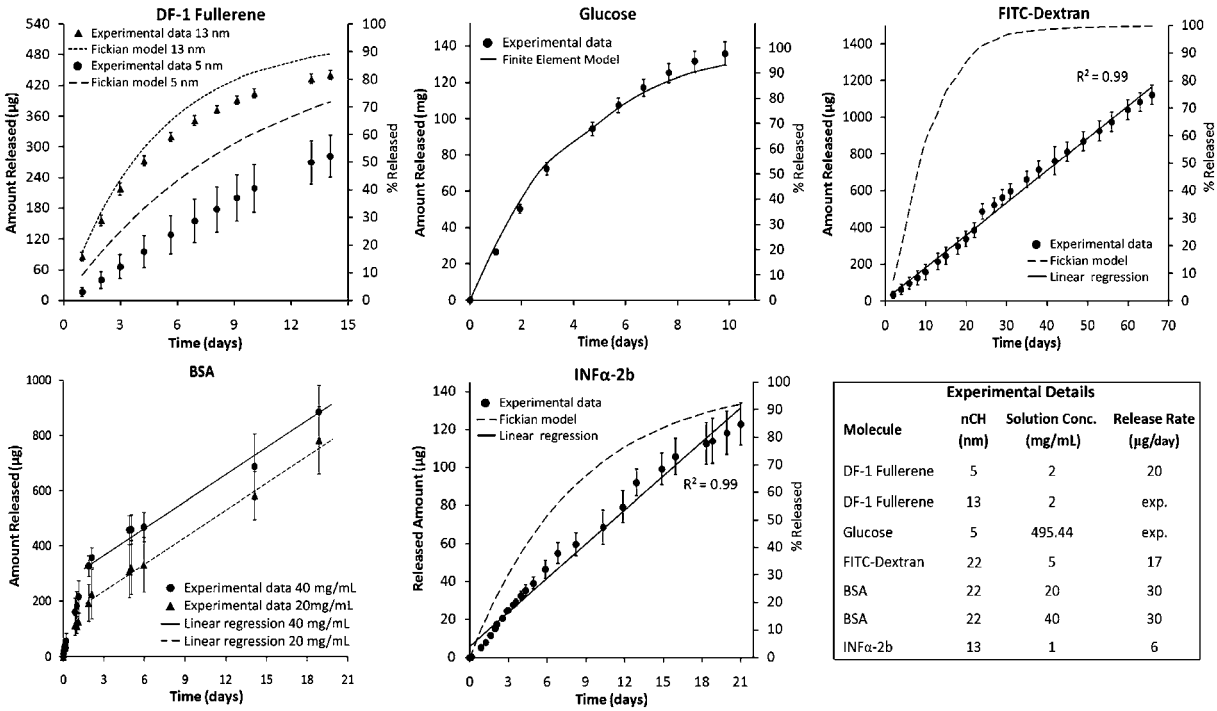

Experimental Details

Molecule	nCH (nm)	Solution Conc. (mg/mL)	Release Rate (μg/day)
DF-1 Fullerene	5	2	20
DF-1 Fullerene	13	2	exp.
Glucose	5	495.44	exp.
FITC-Dextran	22	5	17
BSA	22	20	30
BSA	22	40	30
INFα-2b	13	1	6

Fig. 5 The theoretical and experimental release profiles of the 5 molecules tested in the custom designed diffusion chambers. The analytical calculation for dendritic fullerene 1, fluorescein isothiocyanate conjugated dextran, and interferon α-2b are based on Fickian diffusion (see Table 2 for diffusion constants). For glucose, a numerical calculation based on three dimensional finite element analysis is presented. For bovine serum albumin (BSA), two starting source concentrations of 20 and 40 mg/mL were used which released 26.11 and 14.76%, respectively, with identical release rates (after a stabilization period described in the text). By using both starting concentrations, linear release could be demonstrated for up to 63.05% of the total amount of loaded BSA from the 40 mg/mL solution with an experimental duration of only 21 days (once the release rates were verified to be equivalent) as opposed to the 126 days that would be required given the approximate release rate of 30 μg/day.

manufacture of high nanochannel densities while allowing for the exquisite control over their total number and geometry to optimize the zero-order release for specific applications. The mechanical strength can be independently tuned from the release rate by changing the thickness of the SOI handle wafer. Further enhancement can be realized by modulating the Pyrex or CVD cap thickness and adjusting the macrochannel geometry. The presence of the capping and buried oxide layers bound the nanochannel component of the membrane between two amorphous layers. This may help prevent any crystal defects, should they occur, from propagating which has historically been one of the key limiting factors in the use of silicon as a structural biomedical implant material. Based on the burst test results presented here, the primary device breakdown mode for the current design appears to be fracture of the handle wafer with no significant nanochannel performance degradation detected on the 200 by 200 μm membranes where the nanochannel clusters are located. The nDS*sl* membranes, with a thicker handle wafer thickness than the nDS*ab*, were able to reach the burst test pressure limit of 4.1 MPa. High mechanical rigidity is critical as significant osmotic pressures have been recorded for similar semipermeable passive exchange devices loaded with highly concentrated solutions.[55] The fracture pressure of the membranes reported here are significantly higher than those previously reported for the vertically machined nanochannel membranes (see Table 1). Based on pressure limitations of the experimental apparatus used to test the sandwiched bulk membrane the breakdown pressure has yet to be determined.

The release rates reported for the nDS platform presented here compare quite favorably to those demonstrated for a drug delivery architecture using vertically integrated nanochannel membranes[2] to deliver INFα-2b and BSA and are six to seven orders of magnitude higher than a drug delivery implementation using the sandwiched bulk substrate membrane design[3] (see Table 1). The nDS membrane release rates determined for leuprolide, reported in Grattoni, *et al.*,[56] also compare well with the DUROS® osmotic pump (see Table 1).[13]

It has been demonstrated in the literature that linear constrained release occurs when at least one of the dimensions of a fluidic channel is on the order of the hydrodynamic diameter of the molecule diffusing through it.[54] This results in the confinement of the Brownian motion and a saturation of the mass flux for concentrations above a threshold. Surface interactions play a dominant role in these dynamics.[4,9] Based on our experimental observations, a hydrodynamic diameter-to-nanochannel height ratio, or confinement ratio, of approximately 1 : 3 or higher is required to achieve zero-order release for the molecules investigated. The bulk physical parameters, confinement ratios, and dominate surface interactions for each molecule tested are tabulated in Table 2.

The molecules selected benefit from well characterized behavior as reported in the literature. Given the balance of mass to charge and the possible structural conformations of each

Table 1 Comparison of release rates and burst pressures for several drug release platforms and membrane architectures

Membrane Technology	Nanochannel size (nm)	Interferon α-2b release rate (μg/day)	Bovine Serum Albumin release rate (μg/day)	Leuprolide release rate (μg/day)	Maximum sustainable transmembrane pressure
Perpendicular nanochannel membrane	13	N/A	15.8 μg/day (Martin *et al.*)[2]	N/A	137.9 kPa (Chu *et al.*)[16]
	20	53.6 μg/day@ 37 °C (Martin *et al.*)[2]	N/A	N/A	96.5 kPa (Chu *et al.*)[17]
Sandwiched nanochannel membrane with bulk substrates	100	2.44×10^{-6} μg/day @ 37 °C (Lesinski *et al.*)[3]	N/A	N/A	> 2.76 MPa
DUROS® osmotic pump	N/A			120 μg/day (Viadur®)[13]	N/A
nDS*ab* (release rate for BSA calculated after cross over to zero-order release)	22	N/A	33.2 μg/day for 20mg/mL@ 23 °C 30.7 μg/day for 40mg/mL@ 23 °C	N/A	2.76 MPa (500 μm SOI handle wafer)
nDS*sl*	5	N/A	N/A	100 μg/day (Grattoni *et al.*)[56]	> 4.1 MPa (700 μm SOI handle wafer)
	13	5.9 μg/day@ 23 °C	N/A	Fickian (Grattoni *et al.*)[56]	
	20	29.7 μg/day@ 23 °C (Grattoni *et al.*)[56]	N/A	N/A	

Table 2 Characteristic properties of solutes and confinements[a]

Solute	d, nm	d_{min}, nm	q_{net}, e	Mw, kDa	D_B, cm^2/s	nCH, nm	Ratio	$Ratio_{mod}$	Force
Glc	0.5	0.3	0	0.18	0.67[ref. 60]	5	1 : 10	1 : 8	PhS
D × 10[b]	6.0[ref. 72]	1.0	−1	10	0.07[ref. 73]	22	1 : 3	1 : 2	PhS
DF1[c]	2.5	2.0	−18	2.8	0.07	5	1 : 2	1 : 1	EE
						13	1 : 5	1 : 4	EE
BSA	5.5	4.0	−17	66	0.06	22	1 : 4	1 : 2	PhS
INF	3.2	3.0	−2	19	0.07[ref. 74]	13	1 : 4	1 : 3	PhS

[a] Abbreviations: d - effective size as 2*Rg calculated from molecular structure; d_{min} – lowest dimension of molecule; q_{net} – net formal charge of molecule at pH 7; Mw – molecular mass; D_B – bulk diffusion coefficient at infinite dilution as multiple of 10^{-5}; nCH – nanochannel height; Ratio – molecule size to nanochannel height ratio; $Ratio_{mod}$ – predicted molecule size to nanochannel height ratio including surface adsorption effects; Force – dominant force that constrains diffusion; PhS – physisorption; EE – electrostatic exclusion. [b] dextran size is based on Rg. [c] estimated DF1 diffusion coefficient is based on similar size molecules and our experimental results.

molecule investigated, several different forces are expected to play a role in the mass transport of these analytes through the nanochannels. DF-1, a molecule which has shown promise for the purposes of free radical scavenging after exposure to radiation,[57] has a high surface charge but a low molecular weight. This, coupled with the high negative surface charge density of silicon dioxide, would indicate that electrostatic repulsion from the channel wall is expected to play a dominant role in the diffusion of this molecule through the channels, as schematically represented by the red zones in Fig. 6. Electrostatic forces have fairly long interaction lengths as compared to Van der Waals or hydrophobic interactions, corresponding to the Debye length in electrolytes, and have been investigated in other systems such as confined colloids.[58] Karnik *et al.* has demonstrated the ability to control the diffusion of a charged protein, avidin, through a nanochannel by use of an applied transverse field to modulate the channel surface charge.[59] Since the buffer in the present case is PBS, however, the Debye length is expected to be short requiring thinner channels in order to see the effects of confinement. Therefore, a nanochannel height of 5 nm is needed to observe significant deviation from the predicted Fickian release, as indicated in Fig. 5. We are currently investigating the effects that low ionic strength buffers have on the nanoconfinement of this molecule with preliminary results pointing to the dominance of electrostatic confinement.

Physisorption also plays a dominant role in nanochannel diffusion. This process can be the result of several contributing interactions, including Van der Waals forces, hydrophobic interactions, and entropic considerations.[4,5] The primary effect of this phenomenon is to produce a low mobility domain near the nanochannel wall, as depicted by the grey zones in Fig. 6. Although the charge to mass ratio of DF-1 is too large for this process to play a significant role in its diffusion, physisorption factors heavily in the confined transport of the other molecules investigated.

Glucose has diffusion properties that are well understood in the bulk.[60] A recent study based on molecular dynamics simulations (MDS) performed by our group, hypothesizes that glucose diffusion is significantly altered by the channel surface

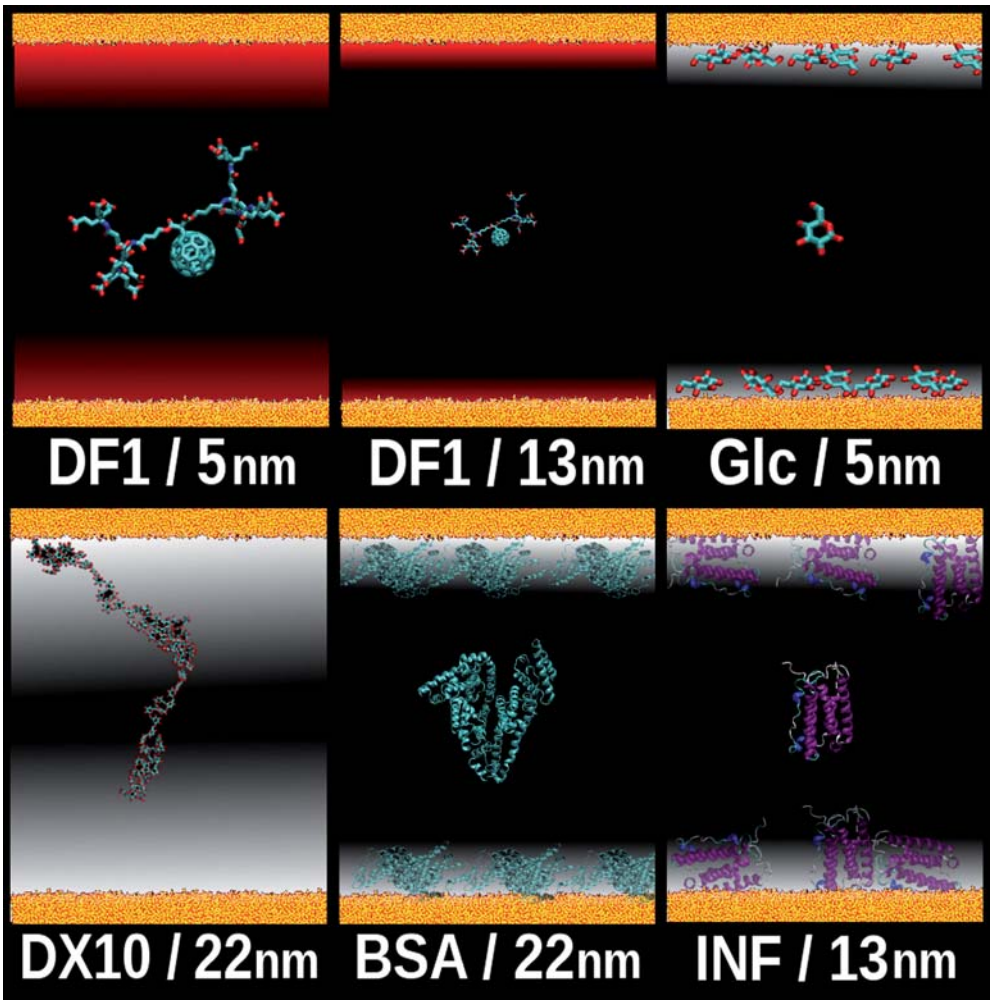

Fig. 6 Pictorial representations of the molecular size to nanochannel height ratios for each analyte tested. The red zones are estimates of the relative electrostatic interaction length between the channel wall and the molecule. The grey zones represent exclusion zones of low mobility due to surface physisorption.

potential and concentrates near the channel wall through physisorption[61] to a thickness of about 0.5 nm. This interaction is mediated by both hydrogen bonding and Van der Waals forces and is reversible with a constant exchange of glucose molecules into and out of the surface-bound layer. However, glucose has also been shown to have a diffusion coefficient which is inversely proportional to concentration.[60] This concentration dependence, accounted for in the FEA, is likely to obscure the confinement effect given the high glucose concentrations used in these experiments, as can be seen in Fig. 5.

The low charge to mass ratio of FITC-dextran, a glucan, indicates that electrostatic forces are minimal. Its structure in bulk solution has been demonstrated to present an extended coil configuration possessing a radius of gyration of 3 nm.[62] Given the large deviation of the theoretical prediction from the experimental data and the sustained zero-order release up to 80% of the initial amount, as shown in Fig. 5, this bulk conformation must certainly by modified by nanoscale confinement. Under certain conditions, dextran has been demonstrated to stretch to almost its full length, approximately 30 nm, as reported under surface saturation conditions.[63] Similar to glucose, dextran has also been shown *via* quartz crystal microbalance measurements on silicon dioxide to have a reversible affinity for hydroxylated surfaces.[64] Dextran would therefore be expected not only to readily adsorb to the silica surface but have a higher affect on nanoscale confinement then its bulk solution conformation would predict, as depicted in Fig. 6.

BSA is a ubiquitous protein used in such chemotherapeutic formulations as Abraxane.[65] Previous work by Martin *et al.* demonstrated constrained release in 13 nm nanochannels and Fickian release in 26 nm nanochannels from a solution at 5 mg/mL[2]. In the present case the initial release of BSA for concentrations of both 20 and 40 mg/mL appears to be concentration gradient dependent, with a confinement ratio of 1 : 4, but transitions to what appears to be constrained after 1.5 days (see Fig. 5). Albumin is known to reversibly adsorb on silicon dioxide but not to agglomerate in solution.[66] It has also been demonstrated that albumin adsorption is dependent on surface preparation protocols, *i.e.* hydroxyl group density and charge.[67] Furthermore, albumin is capable of a conformational change causing enhanced and irreversible adhesion to silicon dioxide.[68–70] As the concentration of albumin in this study is 4 to

8 times higher than in the previous study it seems likely that channel confinement results in local concentrations above the precipitation threshold and further constriction of the nanochannel dimensions. Interestingly, the linearity of the transport behavior after this transition suggests that no additional occlusion occurs and an effective confinement ratio of 1 : 2 is stable. Additional studies are ongoing to understand this observation.

INFα-2b is a molecule used directly in chemotherapy as it can activate the immune response and interrupt viral reproduction.[71] INFα-2b is a globular protein with both hydrophobic and hydrophilic surface domains, similar to BSA, and is influenced by physisorption while under nanoconfinement but did not undergo the irreversible conformational change observed for BSA, as shown in Fig. 5 by a lack of diffusive transport crossover. The mean serum half-lives for INFα-2b in humans are less than 24 h for intramuscular administration and subcutaneous injection and less than 6 h for intravenous infusion.[71] *In vivo* experiments are currently being conducted to investigate whether the nDS can improve upon these time scales and will be reported elsewhere.

Conclusion

In this work an implantable nanofluidic delivery system (nDS) was presented that coupled high mechanical robustness with tunable long-term zero-order release. The release rates achieved from this platform for several molecules, including BSA and INFα-2b, were sufficient to be of therapeutic interest. The reliability of the fabrication protocol and the mechanical stability were demonstrated through convective nitrogen flow. Through nanochannel confinement, molecule to surface interactions were exploited to achieve a sustained zero-order release of high and low MW analytes. In particular, the constant release of DF-1 was achieved by promoting the electrostatic repulsion of the molecules from the channel surface in 5 nm nanochannels. Moreover, zero-order release of BSA, FITC-dextran, and INFα-2b was obtained by taking advantage of physisorption of the molecules on the surface of 22 and 13 nm nanochannels.

The release rates and mechanical integrity determined for these nDS membranes compared quite favorably to other implantable drug delivery technologies presented in the literature[2,3] (see Table 1). A major advantage of this architecture is that the mechanical strength can be independently tuned by changing the thickness of the device and handle layers of the SOI substrate as well as the Pyrex or CVD cap, while the molecular release can be finely tuned with the size, number, and length of the nanochannels. In this context, the on-going development of nanochannels as small as 2 nm will enable the constant release of smaller molecules widening the range of applications of the nDS technology.

Acknowledgements

The authors would like to thank the following commercial, academic, and National Nanotechnology Infrastructure Network (NNIN) entities (see ESI† for list of acknowledged personnel): the Jay Conyers Lab at the University of Texas Medical School for providing the DF-1, Plasma-Therm, LLC., St. Petersburg, FL, for the use of and support on their Versaline Deep Dielectric Etcher, EV Group, Tempe, AZ, for assistance and service with anodic bonding, Ron Kehl Engineering, San Jose, CA, for lapping assistance, the Microelectronics Research Center at the University of Texas at Austin, Austin, TX, the Cleanroom Research Laboratory at the University of Texas at Dallas, Dallas, TX, the Cornell Nanofabrication Facility at Cornell University, Ithaca, NY, the Center for Nanoscale Systems at Harvard University, Cambridge, MA, the Stanford Nanofabrication Facility at Stanford University, Palo Alto, CA, the Center for Nano and Molecular Sciences at the University of Texas at Austin, Austin, TX, and the Texas Advanced Computing Center (TACC) at the University of Texas at Austin for providing HPC resources that have contributed to the research results reported within this paper.

This project has been supported with federal funds from NASA (NNJ06HE06A and NNX08AW91G), Department of Defense (DODW81XWH-09-1-0212), as well as fund from State of Texas Emerging Technology Fund, NanoMedical Systems (NMS), and Alliance of NanoHealth (ANH).

References

1 T. A. Desai, W. H. Chu, G. Rasi, P. Sinibaldi-VallebonaBorboni, G. M. Beattie, A. Hayek, and M. Ferrari, in *Proceedings of SPIE*, San Jose, CA, USA, 1997, pp. 216–226.
2 F. Martin, R. Walczak, A. Boiarski, M. Cohen, T. West, C. Cosentino and M. Ferrari, *J. Controlled Release*, 2005, **102**, 123–133.
3 G. B. Lesinski, S. Sharma, K. A. Varker, P. Sinha, M. Ferrari and W. E. Carson, *Biomed. Microdevices*, 2005, **7**, 71–79.
4 W. Sparreboom, A. Van den Berg and J. C. T. Eijkel, *Nat. Nanotechnol.*, 2009, **4**, 713–720.
5 J. C. T. Eijkel and A. Van den Berg, *Chem. Soc. Rev.*, 2010, **39**, 957–973.
6 S. Pricl, M. Ferrone, M. Fermeglia, F. Amato, C. Cosentino, M. Cheng, R. Walczak and M. Ferrari, *Biomed. Microdevices*, 2006, **8**, 277–290.
7 F. Amato, C. Cosentino, S. Pricl, M. Ferrone, M. Fermeglia, M. Cheng, R. Walczak and M. Ferrari, *Biomed. Microdevices*, 2006, **8**, 291–298.
8 L. Bocquet and E. Charlaix, *Chem. Soc. Rev.*, 2010, **39**, 1073–1095.
9 A. Ziemys, M. Ferrari and C. N. Cavasotto, *J. Nanosci. Nanotechnol.*, 2009, **9**, 6349–6359.
10 J. T. Santini, M. J. Cima and R. Langer, *Nature*, 1999, **397**, 335–338.
11 J. M. Maloney, S. A. Uhland, B. F. Polito, N. F. Sheppard, C. M. Pelta and J. T. Santini, *J. Controlled Release*, 2005, **109**, 244–255.
12 R. Langer and N. A. Peppas, *AIChE J.*, 2003, **49**, 2990–3006.
13 Bayer Pharmaceuticals Corporation and ALZA Corporation, *Viadur Prescribing Information*, 2005, 08840302, R.2.
14 S. H. B. Litster, D. Kim and J. G. Santiago, *P. IMECE*, 2007.
15 A. Grattoni, D. Fine, A. Ziemys, J. Gill, E. Zabre, R. Goodall and M. Ferrari, *Curr. Pharm. Biotechnol.*, 2010, **11**, 343–365.
16 W. H. Chu and M. Ferrari, in Microrobotics and Micromechanical Systems, SPIE, Philadelphia, PA, USA, 1995, vol. 2593, pp. 9–20.
17 W. H. Chu, T. Huen, J. K. Tu, and M. Ferrari, in *Micro- and Nanofabricated Electro-Optical Mechanical Systems for Biomedical and Environmental Applications*, SPIE, San Jose, CA, USA, 1997, vol. 2978, pp. 111–122.
18 J. K. Tu, T. Huen, R. Szema, and M. Ferrari, in *Micro- and Nanofabricated Structures and Devices for Biomedical Environmental Applications*, ed. P. L. Gourley, SPIE, San Jose, CA, USA, 1998, vol. 3258, pp. 148–155.
19 T. A. Desai, D. J. Hansford, L. Leoni, M. Essenpreis and M. Ferrari, *Biosens. Bioelectron.*, 2000, **15**, 453–462.
20 R. Fan, Y. Wu, D. Li, M. Yue, A. Majumdar and P. Yang, *J. Am. Chem. Soc.*, 2003, **125**, 5254–5255.
21 T. S. Kustandi, W. W. Loh, H. Gao and H. Y. Low, *ACS Nano*, 2010, **4**, 2561–2568.
22 S. E. Jones, S. A. Ditner, C. Freeman, C. J. Whitaker and M. A. Lock, *Appl. Environ. Microbiol.*, 1989, **55**, 529–530.

23 H. D. Tong, H. V. Jansen, V. J. Gadgil, C. G. Bostan, E. Berenschot, C. J. M. van Rijn and M. Elwenspoek, *Nano Lett.*, 2004, **4**, 283–287.
24 S. A. Miller, V. Y. Young and C. R. Martin, *J. Am. Chem. Soc.*, 2001, **123**, 12335–12342.
25 Y. Shin and S. Lee, *Nano Lett.*, 2008, **8**, 3171–3173.
26 O. A. Saleh and L. L. Sohn, *Nano Lett.*, 2003, **3**, 37–38.
27 S. J. Kim and J. Han, *Anal. Chem.*, 2008, **80**, 3507–3511.
28 K. P. Nichols, J. C. T. Eijkel and H. J. G. E. Gardeniers, *Lab Chip*, 2008, **8**, 173.
29 S. B. Lee and C. R. Martin, *Anal. Chem.*, 2001, **73**, 768–775.
30 J. Li, D. Stein, C. McMullan, D. Branton, M. J. Aziz and J. A. Golovchenko, *Nature*, 2001, **412**, 166–169.
31 P. Apel, *Radiat. Meas.*, 2001, **34**, 559–566.
32 C. Song and P. Wang, *IEEE Trans. Nanotechnol.*, 2010, **9**, 138–141.
33 Y. Li, Z. Ling, J. Wang, S. Chen, X. Hu and X. He, *Chin. Sci. Bull.*, 2008, **53**, 1608–1612.
34 A. J. Storm, J. H. Chen, X. S. Ling, H. W. Zandbergen and C. Dekker, *Nat. Mater.*, 2003, **2**, 537–540.
35 P. Mao and J. Han, *Lab Chip*, 2005, **5**, 837–844.
36 S. Sharma, A. J. Nijdam, P. M. Sinha, R. J. Walczak, X. Liu, M. M. Cheng and M. Ferrari, *Expert Opin. Drug Delivery*, 2006, **3**, 379–394.
37 G. Voskerician, M. S. Shive, R. S. Shawgo, H. Recum, J. M. Anderson, M. J. Cima and R. Langer, *Biomaterials*, 2003, **24**, 1959–1967.
38 K. E. La Flamme, K. C. Popat, L. Leoni, E. Markiewicz, T. J. La Tempa, B. B. Roman, C. A. Grimes and T. A. Desai, *Biomaterials*, 2007, **28**, 2638–2645.
39 T. A. Desai, W. H. Chu, J. K. Tu, G. M. Beattie, A. Hayek and M. Ferrari, *Biotechnol. Bioeng.*, 1998, **57**, 118–120.
40 T. A. Desai, D. J. Hansford, L. Kulinsky, A. H. Nashat, G. Rasi, J. Tu, Y. Wang, M. Zhang and M. Ferrari, *Biomed. Microdevices*, 1999, **2**, 11–40.
41 P. M. Sinha, G. Valco, S. Sharma, X. Liu and M. Ferrari, *Nanotechnology*, 2004, **15**, S585–S589.
42 W. Fissell, H. Humes, A. Fleischman and S. Roy, *Blood Purif.*, 2007, **25**, 12–17.
43 W. H. Fissell, A. Dubnisheva, A. N. Eldridge, A. J. Fleischman, A. L. Zydney and S. Roy, *J. Membr. Sci.*, 2009, **326**, 58–63.
44 T. A. Desai, D. Hansford and M. Ferrari, *J. Membr. Sci.*, 1999, **159**, 221–231.
45 L. T. Canham, C. L. Reeves, A. Loni, M. R. Houlton, J. P. Newey, A. J. Simons and T. I. Cox, *Thin Solid Films*, 1997, **297**, 304–307.
46 R. Walczak, A. Boiarski, M. Cohen, T. West, K. Melnik, J. Shapiro, S. Sharma and M. Ferrari, *NanoBiotechnology*, 2005, **1**, 35–42.
47 Y. Wang and M. Ferrari, *J. Mater. Sci.*, 2000, **35**, 4923–4930.
48 M. Zhang and M. Ferrari, *Biotechnol. Bioeng.*, 1997, **56**, 618–625.
49 Z. Miqin, T. Desai and M. Ferrari, *Biomaterials*, 1998, **19**, 953–960.
50 P. Mao and J. Han, *Lab Chip*, 2009, **9**, 586–591.
51 F. Laerme, A. Schilp, K. Funk, and M. Offenberg, in *Micro Electro Mechanical Systems, 1999. MEMS '99*. Twelfth IEEE International Conference on, 1999, pp. 211–216.
52 X. Li, T. Abe and M. Esashi, *Sens. Actuators, A*, 2001, **87**, 139–145.
53 A. Grattoni, E. De Rosa, S. Ferrati, Z. Wang, A. Gianesini, X. Liu, F. Hussain, R. Goodall and M. Ferrari, *J. Micromech. Microeng.*, 2009, **19**, 115018.
54 C. Cosentino, F. Amato, R. Walczak, A. Boiarski and M. Ferrari, *J. Phys. Chem. B*, 2005, **109**, 7358–7364.
55 A. Grattoni, G. Canavese, F. M. Montevecchi and M. Ferrari, *Anal. Chem.*, 2008, **80**, 2617–2622.
56 A. Grattoni, H. Shen, D. Fine, A. Ziemys, J. Gill, L. Hudson, S. Hosali, R. Goodall and M. Ferrari, *Pharm. Res.*, 2010, accepted.
57 B. Daroczi, G. Kari, M. F. McAleer, J. C. Wolf, U. Rodeck and A. P. Dicker, *Clin. Cancer Res.*, 2006, **12**, 7086–7091.
58 S. L. Eichmann, S. G. Anekal and M. A. Bevan, *Langmuir*, 2008, **24**, 714–721.
59 R. Karnik, K. Castelino and A. Majumdar, *Appl. Phys. Lett.*, 2006, **88**, 123114–3.
60 J. K. Gladden and M. Dole, *J. Am. Chem. Soc.*, 1953, **75**, 3900–3904.
61 A. Ziemys, A. Grattoni, D. Fine, F. Hussain and M. Ferrari, *J. Phys. Chem. B*, 2010, in press.
62 Amersham Biosciences, *Dextran Fractions*, 2001, 18-1153-41 AA, pp. 1–6.
63 S. Tasker, G. Matthijs, M. C. Davies, C. J. Roberts, E. H. Schacht and S. J. B. Tendler, *Langmuir*, 1996, **12**, 6436–6442.
64 K. D. Kwon, H. Green, P. Bjöörn and J. D. Kubicki, *Environ. Sci. Technol.*, 2006, **40**, 7739–7744.
65 M. R. Green, G. M. Manikhas, S. Orlov, B. Afanasyev, A. M. Makhson, P. Bhar and M. J. Hawkins, *Ann. Oncol.*, 2006, **17**, 1263.
66 C. A. Haynes and W. Norde, *J. Colloid Interface Sci.*, 1995, **169**, 313–328.
67 O. Svensson and T. Arnebrant, *J. Colloid Interface Sci.*, 2010, **344**, 44–47.
68 K. C. Kwok, K. M. Yeung and N. H. Cheung, *Langmuir*, 2007, **23**, 1948–1952.
69 Y. I. Tarasevich, *Theor. Exp. Chem.*, 2001, **37**, 98–102.
70 T. Maruyama, S. Katoh, M. Nakajima and H. Nabetani, *Biotechnol. Bioeng.*, 2001, **75**, 233–238.
71 E. Radwanski, G. Perentesis, S. Jacobs, E. Oden, M. Affrime, S. Symchowicz and N. Zampaglione, *J. Clin. Pharmacol.*, 1987, **27**, 432.
72 C. E. Ioan, T. Aberle and W. Burchard, *Macromolecules*, 2001, **34**, 3765–3771.
73 T. C. Laurent, L. O. Sundelöf, K. O. Wik and B. Wärmegård, *Eur. J. Biochem.*, 1976, **68**, 95–102.
74 D. C. Burke, *Biochem. J.*, 1961, **78**, 556.